JOURNAL OF GEOPHYSICAL RESEARCH, VOL. 104, NO. D8, PAGES 9135–9149, APRIL 27, 1999

Thermal structure of the Arctic summer mesosphere

F.-J. Lübken

Physikalisches Institut der Universität Bonn, Bonn, Germany

Abstract. In the last 10 years a total of 89 falling spheres (FS) have been launched at high latitudes (~70°N) in the summer season between late April and late September. From this experimental technique, densities and temperatures in the mesosphere and upper stratosphere (~95–35 km) are deduced which represent nearly the entire data set regarding the thermal structure in the high-latitude summer mesosphere where optical methods have problems to give reliable results because of the large solar photon background. Some of the launches took place at times in the season where no measurements have been performed before. The seasonal variation of the mean temperatures and densities derived from the FS measurements deviates significantly from the latest empirical models, in particular, in the upper mesosphere during summer. For example, at the summer mesopause (88 km) the FS temperatures are lower by more than 10 K compared to CIRA-1986 in the time period from the beginning of June until the end of August. The thermal structure in the upper mesosphere is rather persistent throughout the core summer months and changes rapidly in the winter-summer transition at mid-May, and vice versa at mid-August. For example, at typical noctilucent cloud altitudes (82 km) the mean temperature is in the range 153±3 K from the beginning of June until mid-August but changes by, typically, 5–10 K per week before and after this period. A comparison of the FS temperatures with the occurrence probability of noctilucent clouds and polar mesosphere summer echoes suggests that the thermal structure is the main controlling factor for these layers, whereas other ingredients required to form aerosol particles, such as water vapor or condensation nuclei, are of secondary importance.

1. Introduction

The first temperature measurements in the high-latitude mesosphere from the early 1960s [*Theon et al.*, 1967] have stimulated many theoretical efforts in the last 40 years to better understand the physics behind the thermal structure of the upper atmosphere. Even today, the very cold summer mesopause of ~130 K and its variation with season is not fully understood in terms of energy sources and sinks, and the coupling to above and below. Various layered phenomena are observed in this region, some of which have been known for many years, for example, noctilucent clouds (NLC), and some of which have been discovered only recently, for example, polar mesosphere summer echoes (PMSE). Recent reviews of the observational and theoretical background of NLCs and PMSEs have been published in the literature [*Gadsden and Schröder*, 1989; *Cho and Röttger*, 1997]. These layers are presumably made up of aerosols which consist mainly of water ice and can exist only at the very low temperatures around the summer mesopause at middle and polar latitudes. The seasonal variation of NLCs and PMSEs is often taken as a proxy for the thermal structure around the mesopause although it is known that other ingredients such as water vapor and condensation nuclei are required to create these layers. The main goal of this paper is to update the data set on the seasonal variation of the thermal structure around the mesopause during summer and to compare it with the occurrence probability of NLCs and PMSEs.

From the observational point of view the high-latitude summer mesosphere (HLSM) is not easy to access: Remote-sensing techniques have problems giving reliable results, mainly because of the large solar photon background. Therefore, rocket borne techniques applying in situ instrumentation provide the majority of the measurements at these altitudes. A review of high-latitude temperature measurements was presented some years ago [*Lübken and von Zahn*, 1991] (hereinafter referred to as LvZ). Many more profiles have been obtained since then, now also covering the months May and September, where no data were available at that time. We will present a summary of nearly all temperature measurements available at high latitudes, concentrating on the

Paper number 1999JD900076.
0148-0227/99/1999JD900076$09.00

months around the summer season, namely, from late April until late September.

In section 2 the in situ measurements and the data analysis procedure are presented. We will compare our results with empirical reference atmospheres taken from the Committee on Space Programs and Research (COSPAR) International Reference Atmosphere (CIRA) and from the latest thermospheric model based on mass spectrometer and incoherent scatter (MSIS) data, hereafter referred to as "CIRA-1986" and "MSIS-1990", respectively [*Fleming et al.*, 1990; *Hedin*, 1991]. In sections 3 and 4 the seasonal variation of temperatures and mass densities in the mesosphere and upper stratosphere is presented. In section 5 we will discuss some sources for a possible systematic bias of our data set, and the implications of the temperature profiles for NLC and PMSE formation.

2. Temperature Measurements in the High-Latitude Summer Mesosphere

2.1. Falling Sphere Technique

We will concentrate on profiles from falling spheres (FS) in this study since nearly all density and temperature measurements in the high-latitude summer mesosphere have been performed applying this technique (see LvZ for a discussion on the very few other measurements applying in situ techniques in the HLSM). The prime quantity determined from the deceleration of the sphere is an atmospheric density profile [*Schmidlin*, 1991]. Temperatures are deduced by (downward) integration of the density profile, assuming hydrostatic equilibrium. The temperature at the upper boundary ("start temperature" T_o) has to be taken from independent measurements or from a model. Fortunately, the influence of T_o on the temperature profile disappears quickly toward lower altitudes: An assumed uncertainty of ±20 K in T_o at 95 km reduces to an uncertainty in the derived temperature profile of ±5, ±2, and <1 K at 90, 87, and <84 km, respectively. In most cases we have used start temperatures from CIRA-1986, unless temperature measurements in the lower thermosphere from the rocket-borne combined neutral and electron (CONE) instrument were available [*Lübken*, 1997a]. The FS technique gives densities and temperatures from ~95 to ~35 km. The height dependent sphere reaction time constant introduces a smoothing of the density and temperature profiles. The smallest scales detectable are typically 8, 3, and 0.8 km at 85, 60, and 40 km, respectively. The uncertainty of the absolute temperature data obtained from the falling sphere is typically 7, 3, and 1.5 K at 90, 80, and 70 km altitude, respectively. A detailed analysis of FS error bars and altitude resolution, as well as an intercomparison with other techniques during winter conditions, is presented in the literature [*Schmidlin*, 1991; *Lübken et al.*, 1994].

As is described in more detail by *Lübken et al.* [1994], the analysis of the FS trajectory requires an initial guess of the atmospheric temperature and density profile (called "reference profiles"), mainly since the drag coefficient of the sphere depends on both Mach and Reynolds numbers, which depend on temperature, density, and sphere velocity. In a second iteration, more realistic Mach and Reynolds numbers are determined from the preliminary temperatures and densities, and so on until the profiles converge. We have taken reference profiles from LvZ for the flights in June and July and CIRA-1986 for the other months (April, May, August, and September). We have modified the pressures listed in CIRA-1986 such that they are in hydrostatic equilibrium with the CIRA-1986 temperature profiles. This modification changes the CIRA-1986 densities by ~10–20% at altitudes between 80 and 110 km. We have tentatively used various reference profiles in the transition months (i.e., LvZ, CIRA-1986, and CIRA-1972 for each month (May and August)) and found that the final temperature profiles are almost independent of the reference profile. For example, for the flight labeled TTS16 performed on August 22, 1997 (which will be discussed in section 2), the data evaluation using the

Table 1. Campaigns Around the Summer Season at High Latitudes With Falling Sphere

Campaign	Period	Number of Flights	Reference
MAC/SINE	June 10–July 19, 1987	25	*von Zahn and Meyer* [1989]
NLC	Aug. 1 – 10, 1991	7	*Goldberg et al.* [1993]
METAL	Sept. 18 – Oct. 3,1991	5	*Alpers et al.* [1993]
AEROSOL-I	April 23 – June 3, 1992	19	this paper
SCALE	July 27–Aug. 1, 1993	4	*Lübken et al.* [1996]
ECHO	July 28–Aug. 17, 1994	9	*Lübken et al.* [1996]
AEROSOL-II	April 2 – May 31, 1995	9	this paper
TRAMP/T	July 15–Sept. 8, 1997	14	this paper

MAC/SINE, Middle Atmosphere Cooperation/Summer in Northern Europe; NLC, noctilucent clouds; METAL, study of metal layers; AEROSOL, study of aerosol layers; SCALE, Scattering Layer Experiment. ECHO indicates that radar and lidar echoes are investigated. TRAMP/T stands for Temperature and Remote Sensing About the Mesopause at Polar Latitudes.

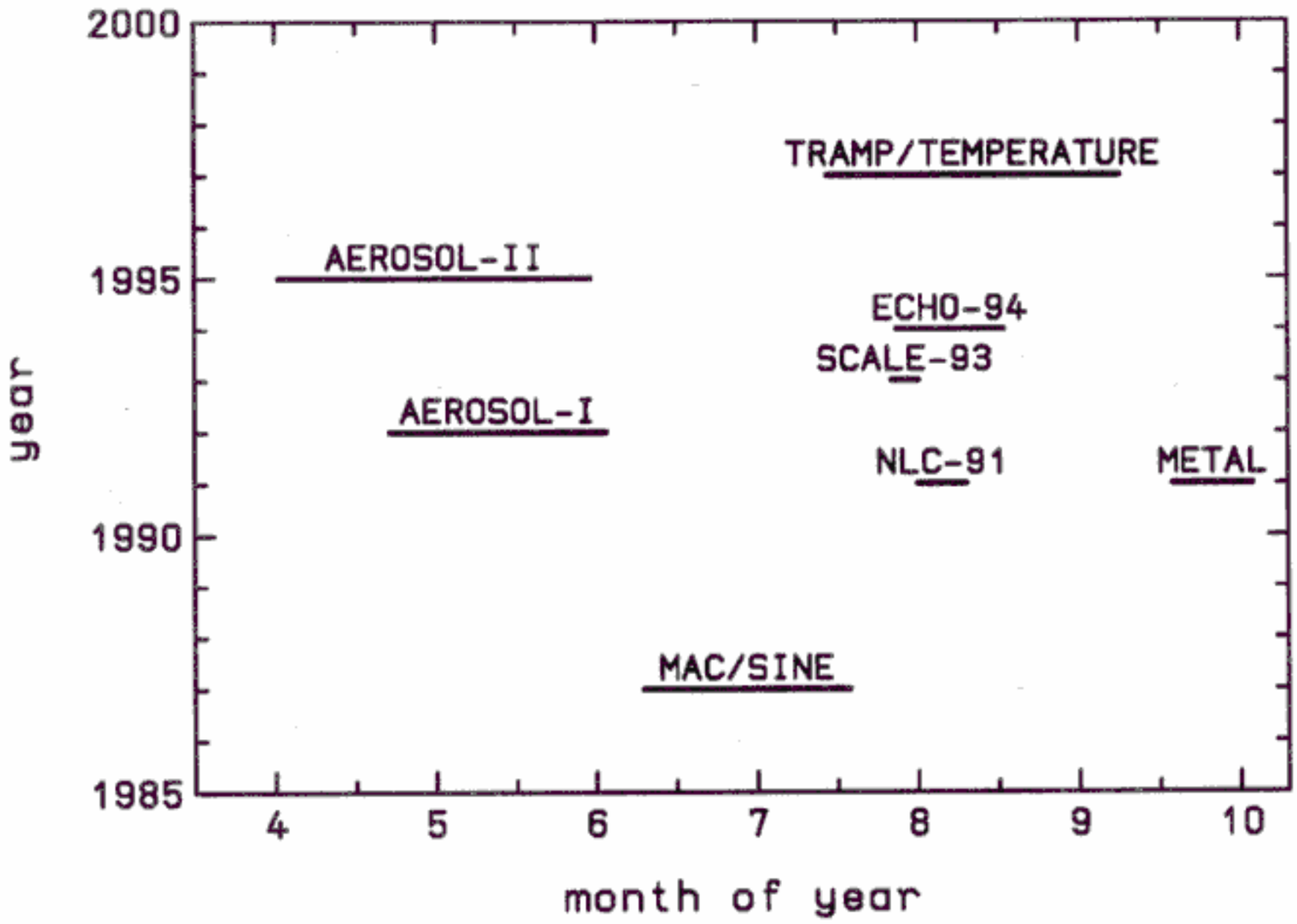

Figure 1. Campaigns around the summer season at high latitudes involving falling sphere measurements. The acronyms are explained in Table 1 and in the text.

LvZ reference from July gave temperatures which are only 1-2 K lower at 80-88 km and only 1-2 K higher at 60-78 km in comparison to the data analysis using the August profile from CIRA-1986. This ensures that the seasonal variation deduced from the FS flights is not somehow prescribed by the reference profile used in the data analysis.

Most rockets used in this study were launched from the Andøya Rocket Range in northern Norway (69°N), and a few flights were performed during the NLC-91 campaign from the Esrange facility close to Kiruna in Sweden (68°N). A list of all campaigns carried out in the last 10 years with FS temperature measurements in the HLSM is presented in Table 1, and the time coverage of each campaign is plotted in Figure 1. A total of 25 FS flights were performed in the scope of the Middle Atmosphere Cooperation/Summer in Northern Europe (MAC/SINE) campaign in 1987 [*von Zahn and Meyer*, 1989] and represented the major database for the compilation in LvZ. In the following years a total of seven campaigns with FS flights took place at high latitudes, now also covering the months adjacent to the core summer months. The total number of FS profiles now available in this period is 89. In section 2.2 we will present individual temperature profiles from those campaigns in Table 1 which have not been presented before in the literature.

2.2. Temperature Profiles From the METAL, AEROSOL, and TRAMP/TEMPERATURE Campaigns

In Figure 2 all temperature profiles measured during the METAL campaign (when metal layers were studied) are shown. The flight dates and times are listed in Table 2. The data from flight LS20 are not further used

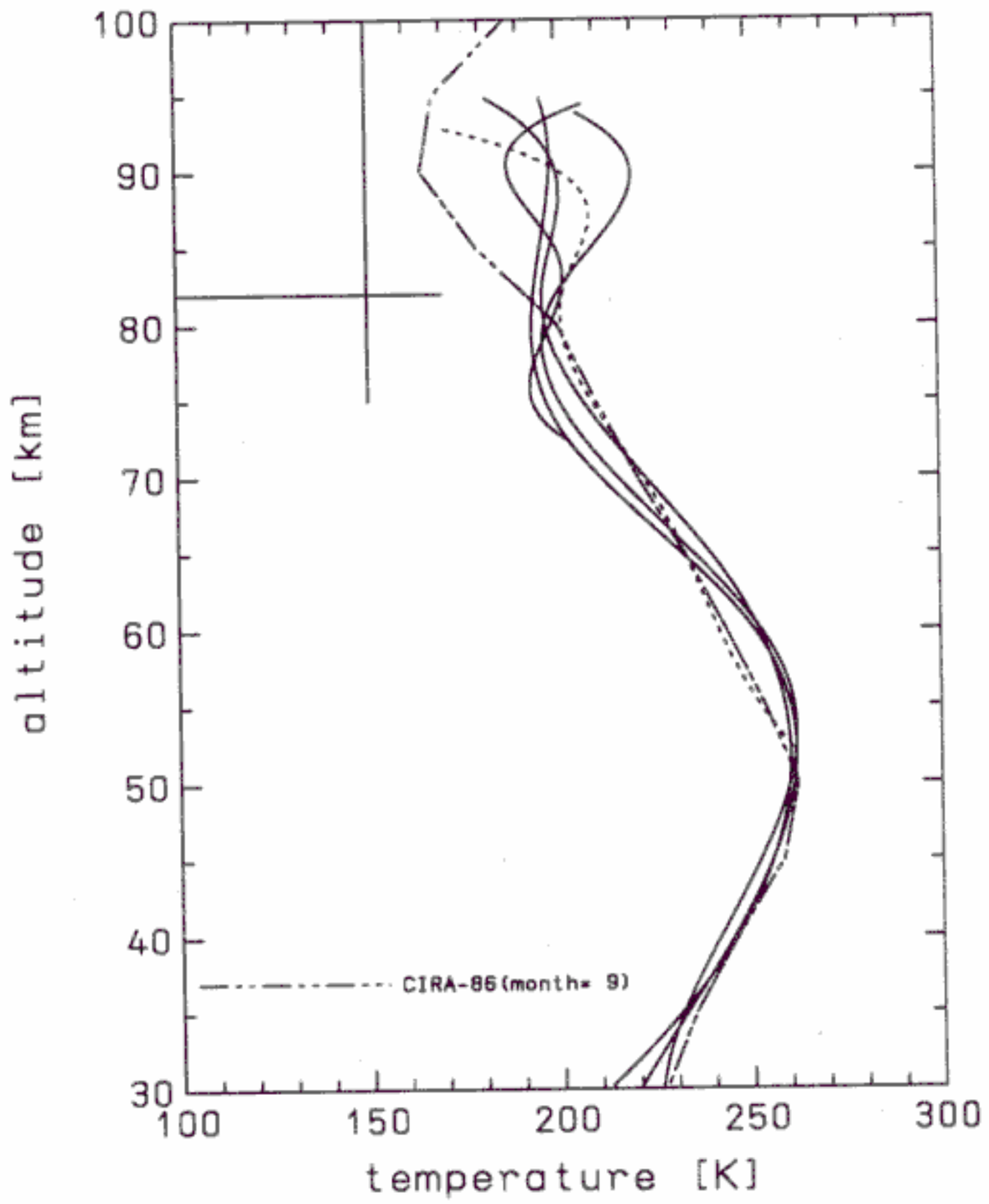

Figure 2. A total of five temperature profiles measured by falling spheres during the METAL campaign from September 17 until October 4, 1991 (see Table 2 for launch dates and times). Note that some of the profiles do not extend into the stratosphere. Flight LS20 (dashed line) is shown for completeness but is not further considered in the paper since it took place in early October, which is too late for the time period studied in this paper. The CIRA-1986 reference profile for September and 70°N is also shown (dashed-dotted line). To facilitate comparison with other plots, the temperature 150 K at an altitude of 82 km has been marked.

Table 2. Falling Sphere Flights During the METAL Campaign in 1991

Flight Label	Date	Time, UT
LS04	Sept. 18	0106:00
LS08	Sept. 20	2130:40
LS11	Sept. 20	2323:30
LS16	Sept. 30	2131:09
LS20	Oct. 3	2316:30

in this paper since it took place in early October, which is too late for the time period considered here. For the METAL flights we have used the start temperature T_o from CONE flights, which took place from the same rocket range within approximately 1 hour of the falling sphere launches. As can be seen from Figure 2, the temperatures in the upper mesosphere are significantly higher compared to CIRA-1986. We have tentatively used T_o from CIRA-1986 and found that this difference does not depend on our choice of T_o (this statement, of course, does not apply at the uppermost 3-4 km where the profiles are close to T_o). Since the METAL flights comprise the only data source in late September, they lead to a corresponding deviation of our mean profiles relative to CIRA-1986 in that period.

Two campaigns called AEROSOL (when aerosol layers were studied) with FS launches were performed in the spring seasons of 1992 and 1995, respectively (flight dates are listed in Table 3 and Table 4, respectively). The individual FS temperature profiles are shown in Figure 3 and Figure 4 (the first two flights during AEROSOL-II are not used since they were performed in the beginning of April, which is too early for the time period considered in this paper). In Figures 3 and 4 the flights before mid-May are plotted differently from those launched later (the separation is not exactly at the same date in both plots because of the spreading of the launch dates). The start temperatures for all flights during AEROSOL-I and AEROSOL-II were taken from CIRA-1986 since no other measurements were available

Table 3. Falling Sphere Flights During the AEROSOL-I Campaign in 1992

Flight Label	Date	Time, UT
AS01	April 23	1430:06
AS02	April 25	1430:21
AS03	April 27	1430:00
AS04	April 29	1430:00
AS05	May 2	1445:27
AS06	May 4	1510:00
AS07	May 6	1450:00
AS08	May 8	1500:00
AS09	May 10	1519:00
AS10	May 12	1510:00
AS13	May 18	1231:30
AS14	May 20	1224:00
AS15	May 22	1430:00
AS16	May 24	1430:00
AS17	May 26	1430:00
AS18	May 28	1430:00
AS19	May 30	1437:00
AS20	June 1	1430:00
AS21	June 3	1430:00

Table 4. Falling Sphere Flights During the AEROSOL-II campaign in 1995

Flight Label	Date	Time, UT
AT01	April 2	2149:00
AT02	April 6	2310:00
AT05	May 4	1100:00
AT06	May 9	1059:00
AT07	May 15	1100:00
AT08	May 20	0001:00
AT09	May 24	2234:00
AT10	May 26	2230:00
AT11	May 31	0036:00

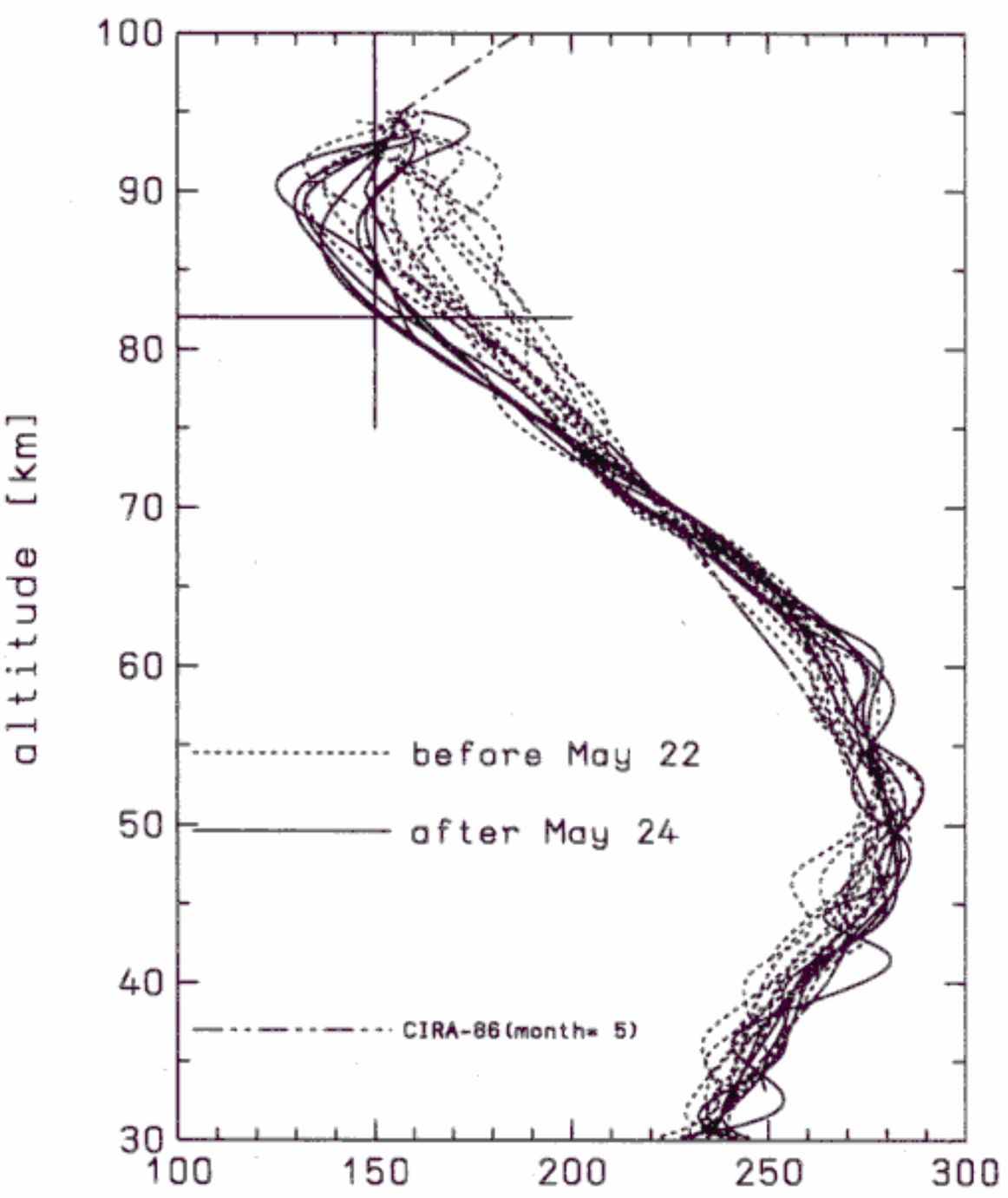

Figure 3. A total of 19 temperature profiles measured by falling spheres during the AEROSOL-I campaign from April 23 until June 3, 1992 (see Table 3 for launch dates and times). Profiles measured before May 22 are plotted with dashed lines, and those measured after May 24 are plotted with solid lines. The CIRA-1986 reference profile for May and 70°N is also shown (dashed-dotted line). The temperature of 150 K at an altitude of 82 km has been marked for comparison reasons.

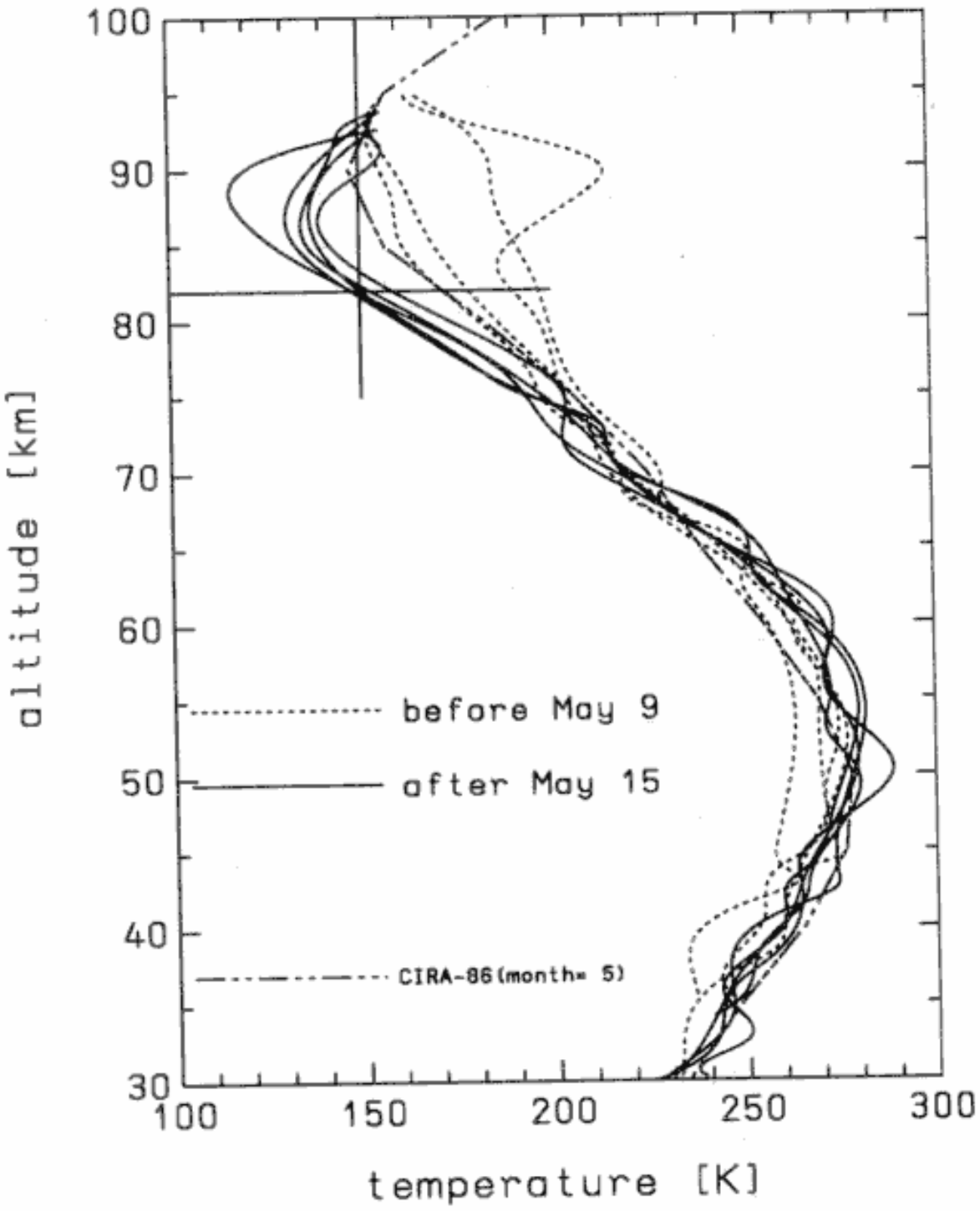

Figure 4. A total of nine temperature profiles measured by falling spheres during the AEROSOL-II campaign from April 2 until May 31, 1995 (see Table 4 for launch dates and times). Profiles measured before May 9 are plotted with dashed lines, and those measured after May 15 are plotted with solid lines. The CIRA-1986 reference profile for May and 70°N is also shown (dashed-dotted line). The temperature of 150 K at an altitude of 82 km has been marked for comparison reasons.

during both campaigns. This explains why all temperatures merge toward the CIRA-1986 reference profiles at the uppermost altitudes (the fact that the FS temperatures at the uppermost altitude do not coincide exactly with CIRA-1986 in some of the profiles in Figure 3 and 4 is due to the fact that different months have been used when retrieving T_o from CIRA-1986, but only one CIRA-1986 profile is shown in Figures 3 and 4). As can be seen from Figures 3 and 4, the temperatures in the upper mesosphere after mid-May are considerably higher compared to early May (for example, at altitudes around 82 km the difference is several tens of Kelvin).

The Temperature and Remote Sensing About the Mesopause at Polar Latitudes (TRAMP)/TEMPERATURE campaign took place in the summer of 1997 at the Andøya Rocket Range. A total of 14 falling spheres were successfully launched in the period from July 15 to September 8 (see Table 5) in close coordination with ground-based measurements of NLCs and PMSEs by the Arctic Lidar Observatory for Middle Atmosphere Research (ALOMAR) facility [*von Zahn*, 1997]. Apart

Table 5. Falling Sphere Flights During the TRAMP/TEMPERATURE Campaign in 1997

Flight Label	Date	Time, UT
TTS01	July 15	1201:37
TTS03	July 21	2120:00
TTS04	July 25	2331:00
TTS05	July 30	2145:00
TTS07	Aug. 4	2328:00
TTS08	Aug. 7	2302:00
TTS09	Aug. 10	2351:00
TTS11	Aug. 14	2000:00
TTS15	Aug. 19	2212:00
TTS16	Aug. 22	1200:00
TTS18	Aug. 26	1226:00
TTS19	Aug. 29	1212:00
TTS22	Sept. 5	1202:00
TTS23	Sept. 8	1204:00

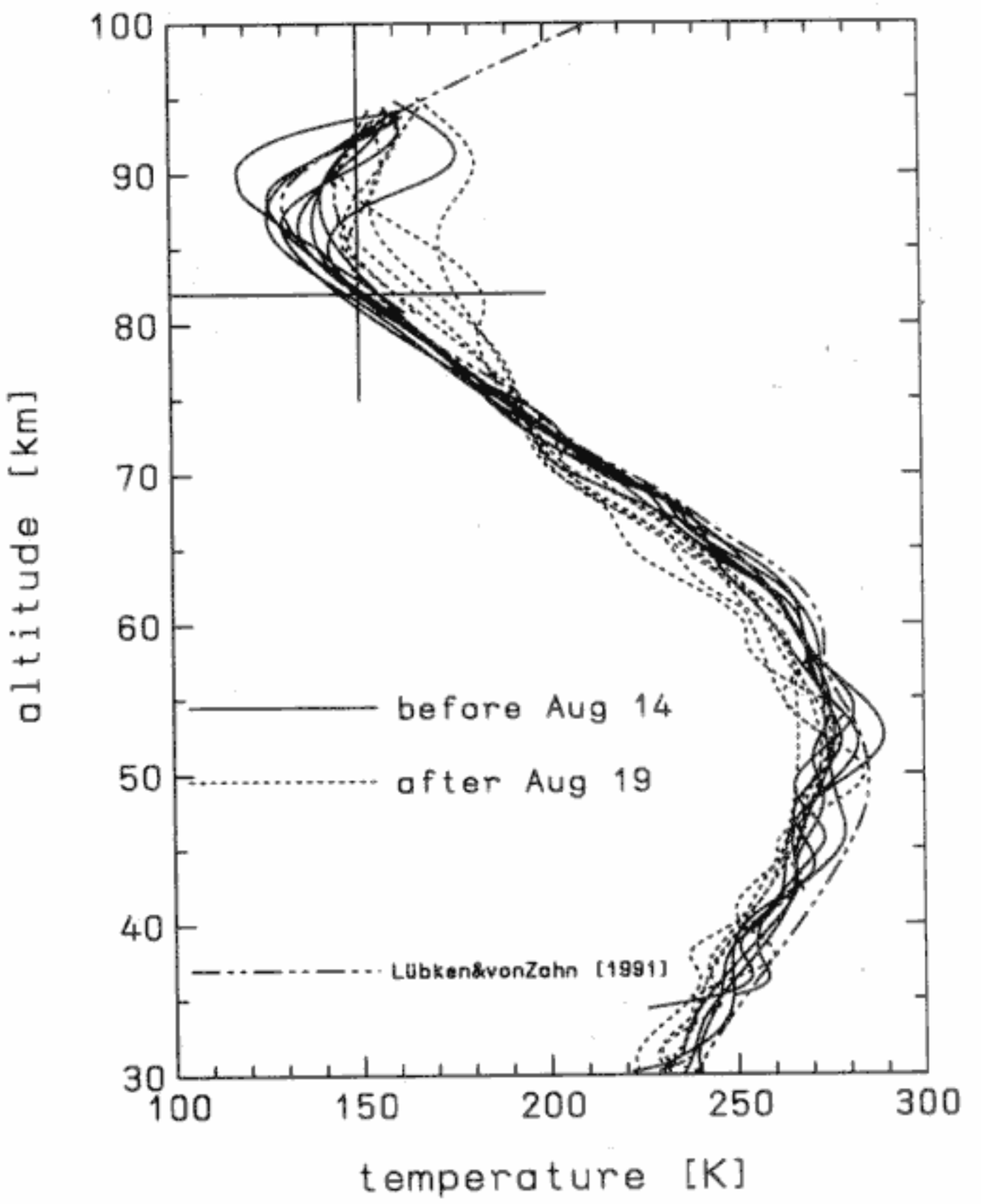

Figure 5. A total of 14 temperature profiles measured by falling spheres during the TRAMP/TEMPERATURE campaign from July 15 until September 8, 1997 (see Table 5 for launch dates and times). Note that some of the profiles do not extend into the stratosphere. Temperatures measured after August 19 are plotted with dashed lines, and those measured before August 14 are plotted with solid lines. The mean profile of July published by *Lübken and von Zahn* [1991] is also shown (dashed-dotted line). The temperature of 150 K at an altitude of 82 km has been marked for comparison reasons.

Table 6. Number of Falling Sphere Flights as a Function of Season

Time Period	Flights
End of April	4
May	20
June	13
July	25
August	21
September	6

The total number of flights is 89.

from the sodium lidar data presented in LvZ, these flights are the first measurements covering the transition from late summer to autumn. We will come back to this transition and to an intercomparison with the Na lidar temperatures in section 5. Individual temperature profiles measured during TRAMP/TEMPERATURE are shown in Figure 5, where the profiles measured before August 14 are plotted differently from those measured later. As can be seen from Figure 5, all "early" profiles are very close to the July mean of LvZ, whereas the temperatures measured after August 19 are significantly higher in the upper mesosphere. For example, at 82 km all "early" profiles are below and all "late" profiles are above 155 K. The FS measurements during TRAMP/TEMPERATURE indicate a rather rapid transition in the upper mesosphere from summer to winter conditions in mid-August (we note that one of the profiles in the early period, namely, TTS08 from August 7th, exhibits a rather large wave like modulation around 90 km; since there is no obvious cause for this unusual behavior, we attribute it to natural variability).

3. Seasonal Variation of Temperatures

Considering all available FS temperature measurements from the end of April until the end of September, a total of 89 flights were performed in the last 10 years. In Table 6 we have listed the number of flights available in each month. We note that more launches took place in the core summer months compared to the transition periods. In order to obtain a seasonal variation of temperatures we have taken all measurements at a given altitude and have calculated the mean temperature in time bins of half a month. This gives a total of 11 data points, which were than smoothed by spline fitting (calculating the spline fit from the raw data, i.e., without preaveraging, would put too much emphasis on the midsummer months). In Figure 6 the individual data points at an altitude of 82 km are shown together with the means over half a month, and the spline fit to the means. Note the rather steep increase of temperature at the end of August and a corresponding decrease in early May. The temperatures change very little and are very close to 150 K from mid-May until mid-August. It was previously noted that this temperature value is surprisingly close to the very first temperature measurements in the early 1960s, and this altitude was therefore called "equithermal submesopause" [*Lübken et al.*, 1996].

The data points and the spline fit in Figure 6 show significant deviations from the CIRA-1986 reference profile, except in the very early and late periods of our measurements. The difference is as much as 10–15 K from June until the end of August. As will be discussed in more detail later, this difference is rather important when studying the relationship between NLC

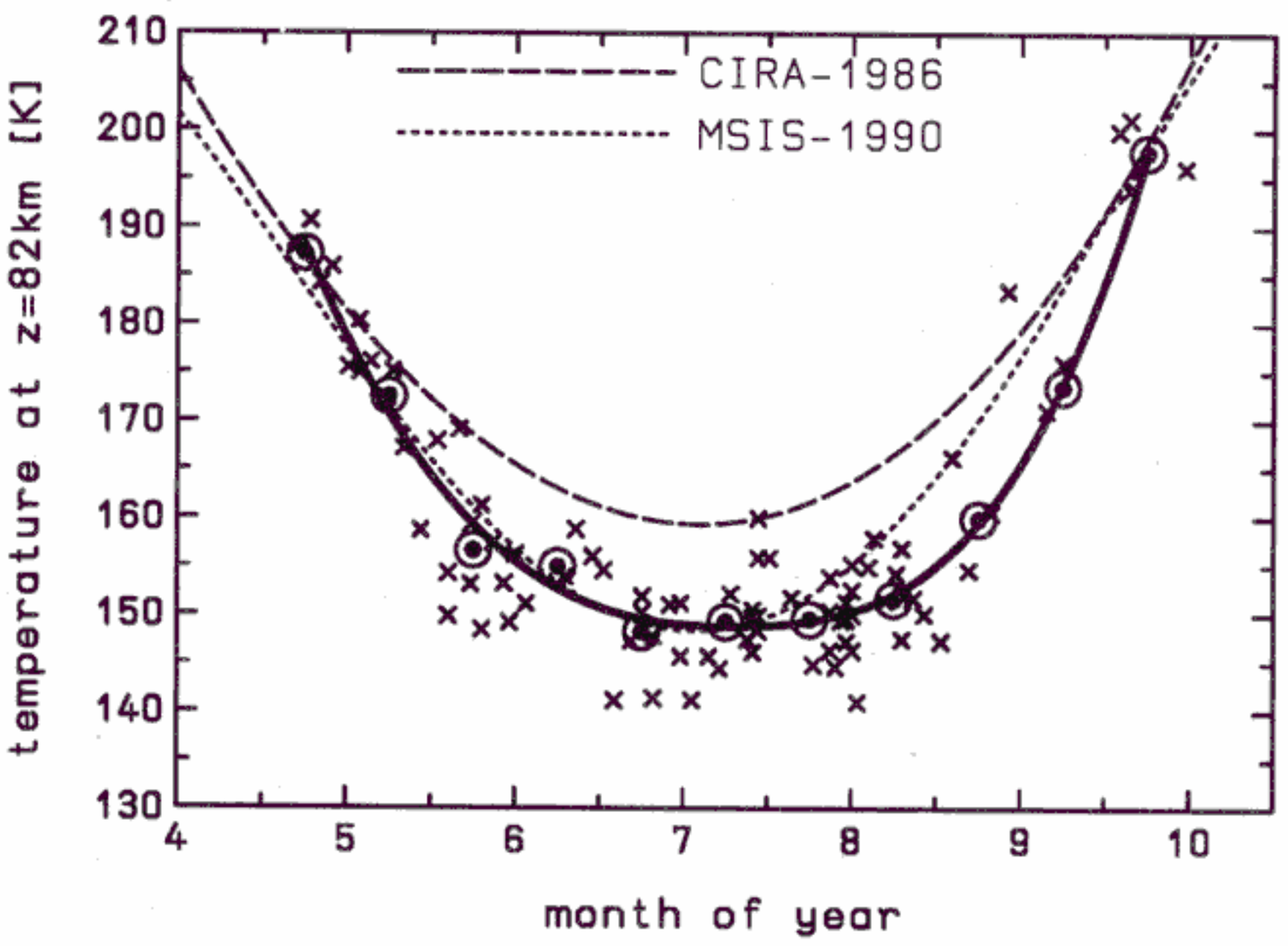

Figure 6. Falling sphere temperatures (crosses) at an altitude of 82 km as a function of season. The FS temperatures have been averaged in time bins of 1 week (dots with circles) and smoothed by spline fitting (thick solid line). Two reference profiles are shown for comparison: CIRA-1986 (long-dashed line) and MSIS-1990 (short-dashed line).

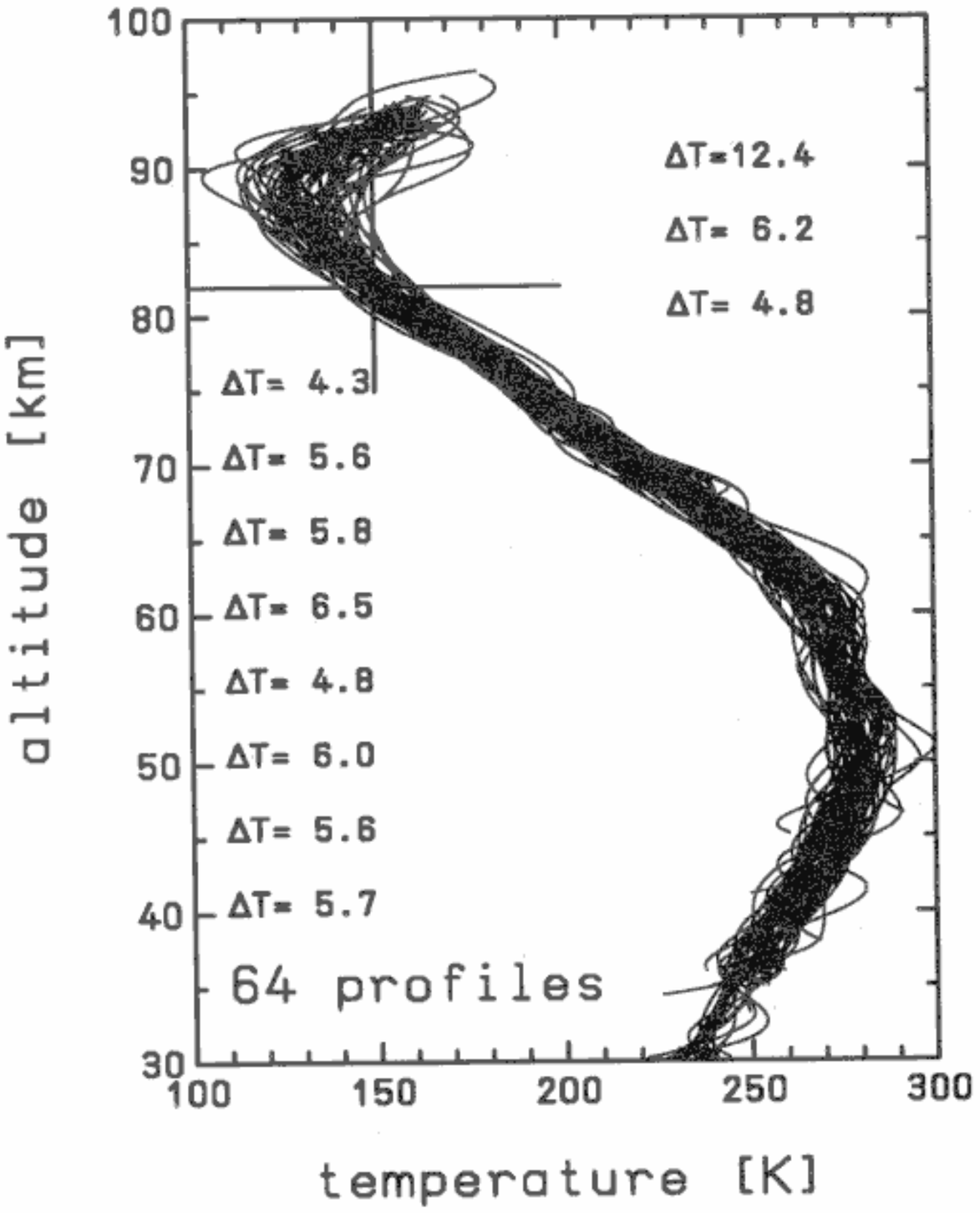

Figure 7. A total of 64 falling sphere temperature profiles observed in the core summer months (here, mid-May until mid-August) in various years. The numbers given at various altitudes indicate the RMS deviation from the mean at that height. The temperature of 150 K at an altitude of 82 km has been marked for comparison reasons.

and/or PMSE occurrence and the thermal structure in the high-latitude summer mesosphere. The MSIS-1990 reference atmosphere seems to represent our FS data better, except during August when MSIS-1990 is too warm by as much as ~10 K.

The steadiness of the thermal structure in the core summer months as observed in Figure 6 is present in the entire altitude range from the upper stratosphere to the upper mesosphere: In Figure 7 we have plotted all individual temperature profiles observed from mid-May until mid-August in various years (1987, 1991, 1992, 1993, 1995, and 1997). As can be seen from Figure 7, the variability is surprisingly small considering that a total of 64 individual temperature profiles are plotted on top of each other. The RMS deviation from the mean is only ~4–6 K in the upper stratosphere and middle mesosphere and increases to ~10–12 K above ~85 km. We have previously noted that the uncertainty of the FS temperatures increases toward the upper end of the profile partly because of the uncertainty caused by the start temperature T_o. Still, the variability is most likely a geophysical effect since it is significantly larger than the uncertainty caused by T_o (see section 2.1). Furthermore, the repeatability of the falling sphere measurements has been demonstrated to be only a few Kelvin, even in the upper mesosphere [see *Lübken et al.*, 1994, Figure 3]. Assuming that the temperature modulations in the atmosphere are caused by dynamical effects, the increase of temperature variability in the upper mesosphere nicely matches the observation that the largest turbulent activity in the summer months occurs at ~87-93 km, whereas turbulence is practically absent at altitudes below ~82 km [*Lübken*, 1997b].

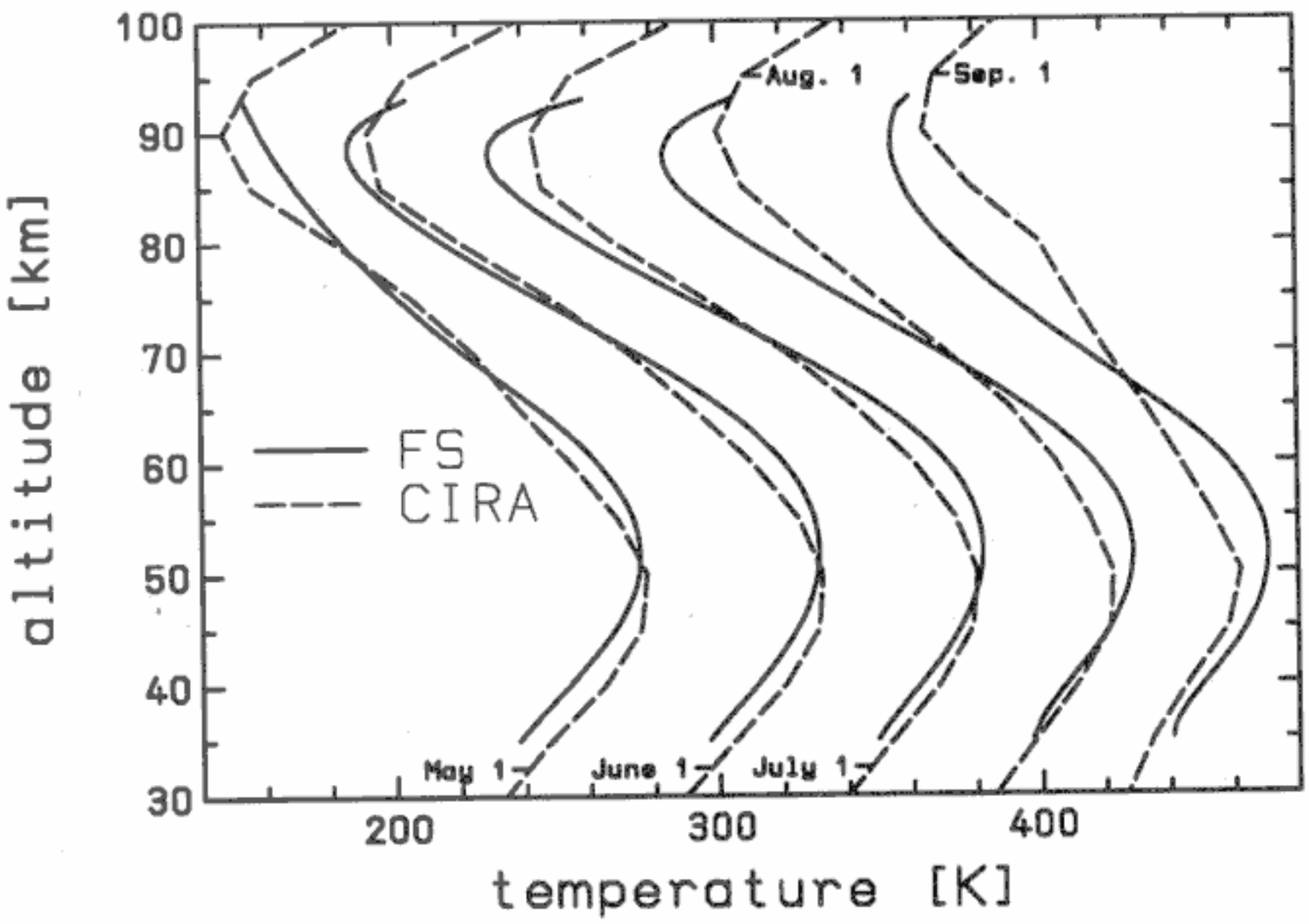

Figure 8. Mean temperature profiles (solid lines) deduced from FS measurements at the beginning of May until the beginning of September. The CIRA-1986 for the corresponding months is shown for comparison (dashed line). The temperature scale is correct only for the May profile; the other profiles have been shifted by 50 K per month. The FS data are taken from Table 7.

Table 7. Seasonal Variation of FS Temperatures

z, km	4.75	5.0	5.25	5.5	5.75	6.0	6.25	6.5	6.75	7.0	7.25	7.5	7.75	8.0	8.25	8.5	8.75	9.0	9.25	9.5	9.75
35	235	238	241	243	245	247	248	249	249	249	249	249	248	247	246	244	242	241	239	236	234
36	237	241	244	246	248	250	251	251	251	251	251	251	250	249	247	245	244	241	239	237	235
37	240	244	247	249	251	253	253	254	254	254	254	253	252	250	249	247	245	243	241	239	236
38	244	247	250	253	254	256	257	257	257	257	256	255	254	253	251	249	247	245	243	241	239
39	247	250	253	256	257	259	260	260	260	260	259	258	257	255	254	252	250	248	246	244	242
40	250	254	256	259	260	262	263	263	263	263	262	261	260	258	256	255	253	251	249	247	245
41	253	257	259	262	263	265	266	266	266	265	265	264	262	261	259	258	256	254	252	250	248
42	257	260	262	264	266	267	268	268	268	268	267	266	265	264	262	260	259	257	255	253	250
43	260	263	265	267	269	270	271	271	271	271	270	269	268	267	265	263	261	259	257	255	253
44	263	265	268	270	271	272	273	273	273	273	272	271	270	269	267	266	264	262	259	257	255
45	265	268	270	272	273	274	275	275	275	275	274	274	273	271	270	268	266	264	261	259	257
46	268	270	272	274	275	276	277	277	277	277	276	276	275	273	272	270	268	266	263	261	258
47	270	272	274	275	277	278	278	278	278	278	278	277	276	275	273	272	270	267	265	262	259
48	271	273	275	277	278	279	279	280	280	280	279	278	277	276	275	273	271	269	266	263	261
49	273	275	276	278	279	280	280	281	281	281	280	280	279	277	276	274	272	269	267	264	261
50	274	275	277	279	280	281	281	281	281	281	281	280	279	278	277	275	273	270	268	265	262
51	274	276	277	279	280	281	282	282	282	282	281	281	280	278	277	275	273	270	268	265	262
52	274	276	278	279	280	281	282	282	282	282	281	281	280	279	277	275	273	271	268	265	262
53	273	275	277	279	280	281	282	282	282	282	281	281	280	278	277	275	273	270	268	265	262
54	273	275	276	278	279	280	281	281	281	281	281	280	279	278	276	274	272	270	267	264	261
55	271	274	275	277	279	280	280	281	281	280	280	279	278	277	275	273	271	269	266	263	260
56	270	272	274	276	277	278	279	279	279	279	279	278	277	275	274	272	270	267	265	262	259
57	268	270	272	274	276	277	278	278	278	278	277	276	275	274	272	270	268	265	263	260	257
58	266	268	270	272	274	275	276	276	276	276	275	274	273	271	270	268	265	263	261	258	255
59	263	266	268	270	272	273	274	274	274	274	273	272	271	269	267	265	263	261	259	256	253
60	260	263	265	267	269	270	271	271	271	271	270	269	268	266	264	262	260	258	256	253	251
61	257	260	262	264	266	267	268	268	268	268	267	266	264	263	261	259	256	255	253	250	248
62	253	256	259	261	263	264	265	265	265	264	263	262	261	259	257	255	253	251	249	247	244
63	249	253	255	257	259	260	261	261	261	260	260	258	257	255	253	251	249	247	245	243	241
64	245	249	251	253	255	256	257	257	257	256	255	254	252	251	249	247	244	243	241	239	237
65	241	244	247	249	251	252	252	252	252	251	250	249	248	246	244	242	240	238	236	234	232
66	236	240	243	244	246	247	247	247	247	246	245	244	243	241	239	237	235	233	231	229	228
67	232	235	238	240	241	242	242	242	242	241	240	239	237	236	234	232	230	228	226	224	223
68	228	231	233	235	236	236	236	236	236	235	234	233	232	230	229	227	225	223	221	219	218
69	224	226	228	230	230	231	231	230	230	229	228	227	226	224	223	222	220	218	217	215	214
70	220	222	223	224	225	225	225	224	224	223	222	221	220	219	217	216	215	214	212	211	210
71	216	217	218	219	219	219	219	218	218	217	216	215	214	213	212	211	210	209	208	207	206
72	213	213	214	214	213	213	212	212	211	210	210	209	208	207	206	205	205	204	204	203	203
73	210	209	209	208	208	207	206	205	205	204	203	202	202	201	200	200	200	199	200	200	201
74	207	205	204	203	202	201	200	199	198	197	197	196	195	195	194	194	195	195	196	197	199
75	204	201	199	198	196	195	193	192	192	191	190	190	189	189	189	189	190	190	192	195	198
76	201	198	195	193	190	189	187	186	185	184	184	183	183	183	183	184	185	186	189	193	197
77	199	194	190	187	185	183	181	180	179	178	178	177	177	177	177	178	180	182	186	191	196
78	196	191	186	182	179	177	175	174	173	172	171	171	171	171	172	173	175	178	183	189	196
79	194	187	182	177	174	171	169	168	167	166	166	166	165	166	167	168	171	174	180	187	196
80	192	184	178	173	169	166	163	162	161	160	160	160	160	160	162	164	167	171	177	186	197
81	190	181	174	168	164	161	158	156	155	155	155	155	154	155	157	159	163	168	175	185	197
82	187	178	170	164	159	156	153	151	150	149	149	149	149	150	152	155	159	165	173	184	198
83	185	175	167	160	155	151	148	146	145	144	144	144	145	146	148	151	155	162	171	183	199
84	183	173	164	157	151	147	144	142	141	140	140	140	140	142	144	147	152	160	170	183	199
85	181	170	161	153	148	143	140	138	136	136	136	136	137	138	141	144	150	158	168	182	200
86	178	168	159	150	144	140	137	134	133	132	132	133	134	136	138	142	147	157	167	182	201
87	176	165	156	148	142	138	134	132	130	130	130	131	132	134	137	140	146	155	166	181	201
88	173	163	155	146	141	136	133	131	129	129	129	130	132	134	136	140	145	155	166	181	202
89	170	161	153	146	140	136	133	131	130	130	130	131	133	135	137	140	145	154	166	181	202
90	167	159	152	146	141	138	135	134	133	133	133	134	136	137	139	142	146	155	166	181	202
91	164	157	151	147	144	141	139	139	139	138	139	140	140	141	142	144	149	155	166	181	201
92	161	155	151	149	148	147	147	147	147	147	147	147	147	147	147	149	152	156	167	181	201
93	156	154	153	153	153	154	156	157	158	159	159	159	157	155	154	154	156	160	168	181	199

Temperatures are in Kelvin. Month of the year: 5.0, May 1; 5.5, May 15; etc.

The spline fit procedure described above has been repeated at all altitudes from 35 km up to 93 km. From the spline functions we have evaluated temperature profiles as a function of altitude at time intervals of ~1 week, starting at May 23 until September 23. These T(z) profiles were again smoothed in order to remove minor "wiggles" in the profiles. In Figure 8 we compare FS temperatures at various times of the year with the corresponding CIRA-1986 values. In general, the FS temperatures are lower in the upper mesosphere compared to CIRA-1986 (except in May) with maximum deviations of up to 15–20 K. In the lower mesosphere, FS temperatures are higher by up to 10 K than CIRA-1986, and in the upper stratosphere the FS means are

again lower than CIRA-1986 (except in September).

The entire data set, that is, the smoothed temperature profiles from 35 to 93 km as a function of season, is listed in Table 7 and is displayed in Plate 1. Note the very cold summer mesopause at ~88 km with temperatures below 130K and the rapid transition from winter to summer in mid-May, and vice versa at the end of August. The mesopause cannot be observed outside the summer months since it is located above the altitude range of the FS technique.

4. Seasonal Variation of Mass Densities

We have applied a similar procedure as described in section 3 to the mass densities $\rho(z)$, or, more precisely, to the logarithm of ρ. The result of this analysis is listed in Table 8. Since the spline fit and smoothing calculations were done independently for temperatures and densities, respectively, we cannot expect the corresponding altitude profiles to be in hydrostatic equilibrium. It turns out, however, that the deviation from a hydrostatic profile is typically less than ±1 K, which is smaller than the uncertainties generated by the limited number of digits given in Table 8.

In Figure 9 the relative deviations of the FS mass densities from CIRA-1986 are shown. Whereas in the upper stratosphere and lower mesosphere the FS densities differ no more than ±5% from CIRA-1986, large deviations of up to –45% are found in the upper mesosphere, in particular, in mid-summer. Such large differences can play an important role when modeling particle sedimentation during PMSE and NLC conditions.

5. Discussion

5.1. Is There Any Systematic Bias in the FS Data?

We will now discuss whether there is any systematic bias in the FS temperatures and densities due to limited data sampling or instrumental effects. Nearly all flights were performed around noon or midnight and therefore at the same phase of the semidiurnal tide. Model calculations suggest that the amplitude of the semidiurnal tide is only 2–3 K in the HLSM and that the diurnal tide is even smaller [*Forbes*, 1982]. We therefore presume that our FS temperatures are representative for daily means and that they are not significantly biased by tides. We note that the flights after August 19 during TRAMP/TEMPERATURE were all performed around 1200UT, whereas the earlier flights were at night. If the diurnal tide is much larger than predicted by the models, this could somewhat modify the transition in late August as presented in Figure 3.

Since the existence of the aerosol particles leading to NLCs and PMSEs is presumably closely related to temperatures, we can tentatively take their occurrence variation during the day as an indication for a corresponding modulation of the thermal structure in the HLSM, ignoring for the moment that the appearance of PMSEs and NLCs is dependent on a rather complicated physical process involving various atmospheric parameters, such as water vapor, condensation nuclei, and plasma densities (important for particle charging). PMSEs have a slightly increased occurrence probability around noon compared to the rest of the day [*Williams et al.*, 1996; *Hoffmann et al.*, 1997], whereas the NLCs as observed by lidars show a semidiurnal modulation with peaks around 0600 and 2000 LT [*von Zahn et al.*, 1998]. If the PMSE and NLC modulation is entirely caused by thermal tides, our FS temperatures would be biased toward too high temperatures. We note that one of the most important features of the seasonal variation of the thermal structure in the HLSM, namely, the long and persistent low temperatures from mid-May until mid-August, is independent of any tidal modulation since many of the profiles in that period have been measured at approximately the same local time.

Some of the flights in July and August have been performed after having waited for PMSEs and/or for NLCs and could therefore be biased toward too low temperatures. However, the temperatures during the confirmed absence of these layers do not show any systematic deviation from the mean and are all significantly lower than the empirical models.

Is there any systematic effect in the FS technique itself resulting in too high or too low temperatures? A comparison of falling sphere measurements with various other techniques was performed during winter conditions in the scope of the Dynamics Adapted Network for the Atmosphere (DYANA) campaign [*Lübken et al.*, 1994]. It was found that the measurements of the various techniques are reliable and that the error bars given are realistic. There was a tendency for the FS temperatures at ~68 and 73–77 km to be lower than the Rayleigh lidar values by ~5 K. If these differences are solely caused by the FS technique (ignoring the potential systematic uncertainties of the lidar), the mean profile shown in Plate 1 would be closer to CIRA-1986 at these altitudes.

5.2. Comparison With Sodium Lidar Measurements

The only temperature data available in the second half of August measured before the FS profiles presented in this paper are the sodium lidar measurements summarized by LvZ (their Figure 14). The Na temperatures are significantly higher compared to FS, in particular, in the second half of the month when the sodium lidar mesopause temperature is ~170 K at an altitude of 88 km, whereas the FS mesopause is at the same altitude but is as cold as 140–145 K. We note that the sodium lidar measurements are particularly difficult to perform in the summer season when sodium is less abundant than in winter, and when the solar photon

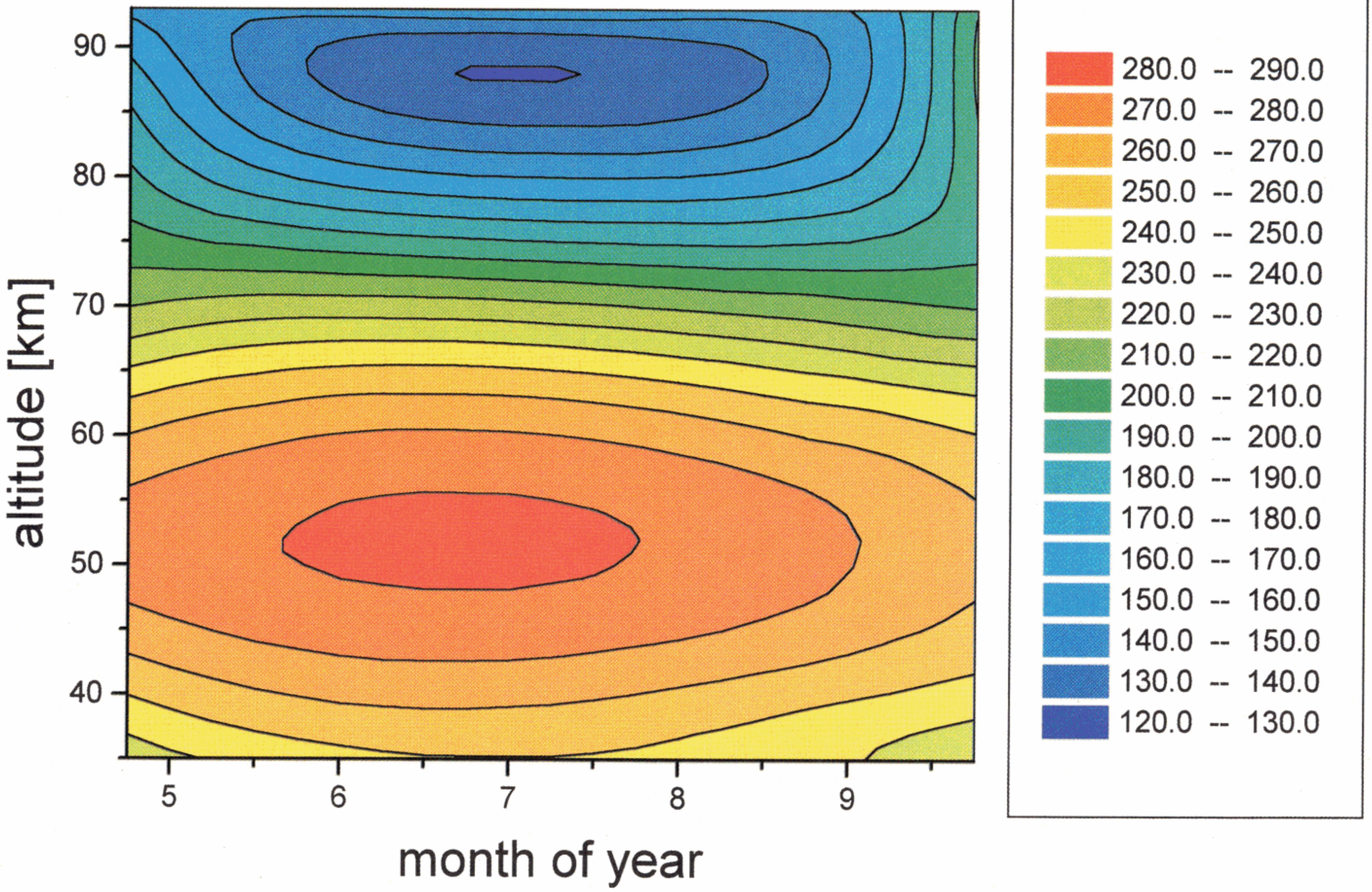

Plate 1. Contour plot of the seasonal variation of mean falling sphere temperatures from April 23 until September 23. The FS temperatures are taken from Table 7. The color code is explained in the insert (values in Kelvin).

Table 8. Seasonal Variation of FS Mass Densities

z, km	4.75	5.0	5.25	5.5	5.75	6.0	6.25	6.5	6.75	7.0	7.25	7.5	7.75	8.0	8.25	8.5	8.75	9.0	9.25	9.5	9.75
35	2.07	2.06	2.06	2.05	2.05	2.05	2.04	2.04	2.03	2.03	2.03	2.03	2.03	2.03	2.04	2.04	2.05	2.06	2.07	2.08	2.09
36	2.13	2.13	2.12	2.12	2.11	2.11	2.11	2.10	2.10	2.09	2.09	2.09	2.09	2.09	2.10	2.10	2.11	2.12	2.13	2.15	2.16
37	2.20	2.19	2.19	2.18	2.18	2.17	2.17	2.16	2.16	2.15	2.15	2.15	2.15	2.15	2.16	2.16	2.17	2.18	2.20	2.21	2.23
38	2.26	2.26	2.25	2.25	2.24	2.23	2.23	2.22	2.22	2.22	2.21	2.21	2.21	2.22	2.22	2.23	2.23	2.25	2.26	2.28	2.30
39	2.33	2.32	2.32	2.31	2.30	2.30	2.29	2.29	2.28	2.28	2.28	2.28	2.28	2.28	2.28	2.29	2.30	2.31	2.33	2.35	2.37
40	2.39	2.39	2.38	2.37	2.37	2.36	2.35	2.35	2.34	2.34	2.34	2.34	2.34	2.34	2.35	2.35	2.36	2.38	2.39	2.41	2.43
41	2.46	2.45	2.44	2.43	2.42	2.42	2.41	2.40	2.40	2.40	2.40	2.40	2.40	2.40	2.41	2.41	2.42	2.44	2.45	2.47	2.49
42	2.52	2.51	2.50	2.49	2.48	2.48	2.47	2.46	2.46	2.46	2.46	2.46	2.46	2.46	2.47	2.47	2.49	2.50	2.52	2.54	2.56
43	2.58	2.57	2.56	2.55	2.55	2.54	2.53	2.52	2.52	2.52	2.52	2.52	2.52	2.52	2.53	2.54	2.55	2.56	2.58	2.60	2.62
44	2.64	2.63	2.62	2.61	2.60	2.60	2.59	2.58	2.58	2.57	2.57	2.57	2.58	2.58	2.59	2.60	2.61	2.62	2.64	2.66	2.68
45	2.70	2.69	2.68	2.67	2.66	2.65	2.64	2.64	2.63	2.63	2.63	2.63	2.63	2.64	2.64	2.65	2.66	2.68	2.70	2.72	2.74
46	2.76	2.75	2.74	2.73	2.71	2.71	2.70	2.69	2.69	2.68	2.68	2.68	2.69	2.69	2.70	2.71	2.72	2.74	2.76	2.78	2.80
47	2.82	2.81	2.80	2.78	2.77	2.76	2.76	2.75	2.74	2.74	2.74	2.74	2.74	2.75	2.76	2.77	2.78	2.80	2.82	2.84	2.86
48	2.88	2.86	2.85	2.84	2.83	2.82	2.81	2.80	2.80	2.80	2.80	2.80	2.80	2.81	2.81	2.82	2.84	2.85	2.87	2.89	2.92
49	2.93	2.92	2.90	2.89	2.88	2.87	2.86	2.86	2.85	2.85	2.85	2.85	2.85	2.86	2.87	2.88	2.89	2.91	2.93	2.95	2.97
50	2.99	2.97	2.96	2.94	2.93	2.92	2.91	2.91	2.90	2.90	2.90	2.90	2.90	2.91	2.92	2.93	2.95	2.96	2.98	3.01	3.03
51	3.04	3.03	3.01	3.00	2.99	2.98	2.97	2.96	2.96	2.96	2.96	2.95	2.96	2.96	2.97	2.98	3.00	3.02	3.04	3.07	3.09
52	3.10	3.08	3.07	3.05	3.04	3.03	3.02	3.02	3.01	3.01	3.01	3.01	3.01	3.02	3.03	3.04	3.06	3.07	3.10	3.12	3.15
53	3.15	3.13	3.12	3.11	3.09	3.08	3.07	3.07	3.06	3.06	3.06	3.06	3.06	3.07	3.08	3.09	3.11	3.13	3.15	3.17	3.20
54	3.20	3.18	3.17	3.15	3.14	3.13	3.12	3.12	3.11	3.11	3.11	3.11	3.11	3.12	3.13	3.14	3.16	3.18	3.20	3.23	3.26
55	3.25	3.24	3.22	3.21	3.19	3.18	3.17	3.17	3.16	3.16	3.16	3.16	3.16	3.17	3.18	3.19	3.21	3.23	3.26	3.29	3.32
56	3.30	3.29	3.27	3.26	3.25	3.24	3.23	3.22	3.21	3.21	3.21	3.21	3.21	3.22	3.23	3.25	3.26	3.29	3.31	3.34	3.37
57	3.35	3.34	3.32	3.31	3.30	3.29	3.28	3.27	3.26	3.26	3.26	3.26	3.27	3.27	3.28	3.30	3.32	3.34	3.36	3.39	3.42
58	3.40	3.39	3.37	3.36	3.35	3.34	3.33	3.32	3.31	3.31	3.31	3.31	3.32	3.32	3.33	3.35	3.37	3.39	3.41	3.44	3.48
59	3.45	3.44	3.42	3.41	3.39	3.38	3.38	3.37	3.36	3.36	3.36	3.36	3.37	3.37	3.38	3.40	3.42	3.44	3.46	3.50	3.53
60	3.51	3.49	3.48	3.46	3.44	3.43	3.42	3.42	3.41	3.41	3.41	3.41	3.41	3.42	3.43	3.45	3.47	3.49	3.52	3.55	3.58
61	3.56	3.54	3.53	3.51	3.50	3.48	3.47	3.46	3.46	3.46	3.46	3.46	3.46	3.47	3.48	3.50	3.52	3.54	3.57	3.60	3.63
62	3.61	3.59	3.58	3.56	3.55	3.53	3.52	3.52	3.51	3.51	3.51	3.51	3.51	3.52	3.53	3.55	3.57	3.59	3.62	3.65	3.68
63	3.66	3.64	3.63	3.61	3.60	3.58	3.57	3.57	3.56	3.56	3.56	3.56	3.56	3.57	3.59	3.60	3.62	3.64	3.67	3.70	3.74
64	3.71	3.69	3.67	3.66	3.64	3.63	3.62	3.61	3.61	3.61	3.61	3.61	3.61	3.62	3.63	3.65	3.67	3.69	3.72	3.75	3.79
65	3.77	3.75	3.72	3.71	3.69	3.68	3.67	3.66	3.66	3.66	3.66	3.65	3.66	3.67	3.68	3.70	3.72	3.75	3.77	3.81	3.84
66	3.82	3.80	3.78	3.76	3.75	3.73	3.72	3.71	3.70	3.70	3.70	3.70	3.71	3.72	3.74	3.75	3.78	3.80	3.83	3.86	3.89
67	3.87	3.85	3.83	3.81	3.80	3.78	3.77	3.76	3.76	3.75	3.75	3.76	3.76	3.78	3.79	3.81	3.83	3.85	3.88	3.91	3.95
68	3.93	3.90	3.88	3.86	3.85	3.83	3.82	3.81	3.81	3.80	3.81	3.81	3.82	3.83	3.84	3.86	3.88	3.91	3.94	3.97	4.01
69	3.98	3.96	3.94	3.92	3.90	3.88	3.87	3.86	3.86	3.86	3.86	3.86	3.87	3.88	3.89	3.91	3.94	3.96	4.00	4.03	4.07
70	4.04	4.01	3.99	3.97	3.95	3.94	3.92	3.91	3.91	3.91	3.91	3.91	3.92	3.93	3.95	3.97	3.99	4.02	4.06	4.09	4.14
71	4.10	4.07	4.05	4.03	4.01	3.99	3.98	3.97	3.96	3.96	3.96	3.97	3.97	3.99	4.01	4.03	4.05	4.08	4.12	4.16	4.20
72	4.16	4.13	4.11	4.08	4.06	4.05	4.03	4.02	4.02	4.01	4.02	4.02	4.03	4.05	4.06	4.09	4.11	4.14	4.18	4.22	4.26
73	4.22	4.19	4.16	4.14	4.12	4.10	4.09	4.08	4.08	4.07	4.07	4.08	4.09	4.11	4.12	4.14	4.17	4.20	4.24	4.28	4.33
74	4.29	4.26	4.22	4.20	4.18	4.16	4.15	4.14	4.13	4.13	4.13	4.14	4.15	4.16	4.18	4.21	4.24	4.27	4.31	4.35	4.40
75	4.35	4.32	4.29	4.26	4.24	4.22	4.21	4.20	4.19	4.19	4.19	4.20	4.21	4.23	4.25	4.27	4.30	4.34	4.38	4.42	4.47
76	4.42	4.38	4.35	4.33	4.30	4.28	4.27	4.26	4.26	4.26	4.26	4.26	4.28	4.29	4.31	4.34	4.37	4.41	4.45	4.49	4.54
77	4.48	4.45	4.42	4.39	4.37	4.35	4.34	4.33	4.32	4.32	4.32	4.33	4.34	4.36	4.38	4.41	4.44	4.47	4.51	4.56	4.61
78	4.55	4.52	4.49	4.46	4.43	4.41	4.40	4.39	4.39	4.39	4.39	4.40	4.41	4.43	4.45	4.48	4.51	4.55	4.59	4.63	4.68
79	4.62	4.59	4.55	4.53	4.50	4.49	4.47	4.46	4.46	4.46	4.46	4.47	4.48	4.50	4.52	4.55	4.58	4.62	4.66	4.71	4.76
80	4.69	4.66	4.63	4.60	4.58	4.56	4.55	4.53	4.53	4.53	4.53	4.55	4.56	4.57	4.60	4.63	4.66	4.69	4.74	4.78	4.83
81	4.76	4.73	4.70	4.67	4.65	4.63	4.62	4.61	4.61	4.61	4.61	4.62	4.64	4.65	4.68	4.70	4.74	4.77	4.81	4.86	4.90
82	4.83	4.80	4.77	4.75	4.73	4.71	4.70	4.69	4.69	4.69	4.70	4.70	4.72	4.73	4.76	4.78	4.82	4.85	4.89	4.93	4.98
83	4.91	4.88	4.85	4.83	4.81	4.79	4.78	4.78	4.77	4.78	4.78	4.79	4.80	4.82	4.84	4.87	4.90	4.93	4.97	5.01	5.05
84	4.98	4.95	4.93	4.91	4.89	4.88	4.87	4.86	4.86	4.86	4.87	4.88	4.89	4.91	4.93	4.95	4.98	5.01	5.05	5.09	5.13
85	5.05	5.03	5.01	4.99	4.98	4.97	4.96	4.95	4.96	4.96	4.96	4.97	4.99	5.00	5.02	5.04	5.07	5.10	5.13	5.16	5.20
86	5.13	5.11	5.09	5.08	5.07	5.06	5.05	5.05	5.05	5.05	5.06	5.07	5.08	5.10	5.12	5.14	5.16	5.18	5.21	5.24	5.28
87	5.20	5.19	5.18	5.17	5.16	5.16	5.15	5.15	5.15	5.16	5.16	5.17	5.18	5.20	5.21	5.23	5.25	5.27	5.30	5.32	5.35
88	5.28	5.28	5.27	5.26	5.26	5.26	5.26	5.26	5.26	5.26	5.27	5.28	5.29	5.30	5.32	5.33	5.35	5.37	5.38	5.40	5.42
89	5.36	5.36	5.36	5.36	5.36	5.36	5.36	5.37	5.37	5.38	5.39	5.39	5.40	5.41	5.42	5.43	5.45	5.46	5.47	5.48	5.50
90	5.44	5.45	5.45	5.45	5.46	5.47	5.47	5.48	5.49	5.49	5.50	5.51	5.52	5.53	5.53	5.54	5.55	5.55	5.56	5.57	5.57
91	5.52	5.53	5.55	5.56	5.57	5.58	5.59	5.60	5.61	5.62	5.63	5.63	5.64	5.64	5.64	5.65	5.65	5.65	5.65	5.64	5.64
92	5.60	5.62	5.64	5.66	5.68	5.70	5.72	5.73	5.74	5.75	5.76	5.76	5.76	5.76	5.76	5.76	5.76	5.75	5.74	5.73	5.72
93	5.68	5.71	5.74	5.78	5.80	5.83	5.85	5.86	5.88	5.89	5.89	5.90	5.90	5.89	5.89	5.88	5.87	5.85	5.83	5.81	5.78

Read 2.07 as $10^{-2.07}\,kg/m^3$. Month of the year: 5.0, May 1; 5.5, May 15; etc.

background is high. Typical instrumental uncertainties are 5–10 K under these unfavorable conditions. We have studied the difference between the FS and the Na profiles in more detail by going back to the original sodium temperature profiles and calculating nightly means. A total of 18 nights with Na temperatures in August are available: 8 in 1986 (in the period 9.–25.), 5 in 1987 (5.–14.), and 7 in 1989 (5.–15.). Unfortunately, there are no simultaneous FS flights available in any of these periods. Whereas the nightly means of the years 1987 and

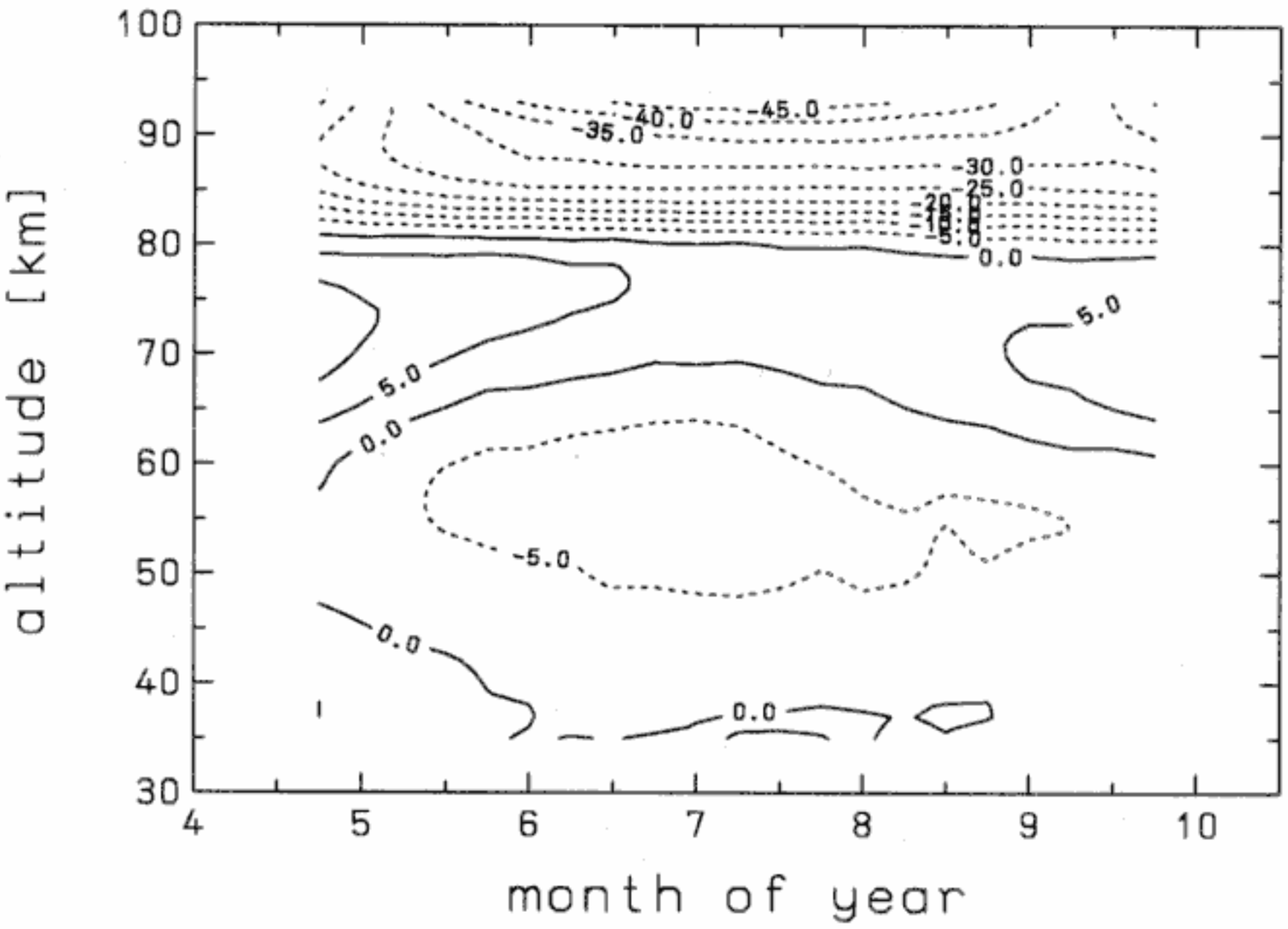

Figure 9. Seasonal variation of the relative difference (in percent) between the falling sphere mass densities and the corresponding CIRA-1986 values at 70°N. Negative values indicate that the FS densities are lower compared to CIRA-1986. The FS data are taken from Table 8.

1989 are in fair agreement with the FS mean, all the Na temperatures from 1986 are systematically higher by as much as 25 K. We note that the summer of 1986 was the first summer season for that particular sodium lidar instrument, which certainly adds to the overall uncertainty of that technique in that year. Although there is considerable scepticism about the sodium lidar temperatures in August 1986, we cannot exclude at the moment that there is a geophysical reason behind the deviation and that the transition in August 1986 occurred indeed some weeks earlier (with corresponding higher temperatures) compared to the other years.

5.3. Implications for PMSE and NLC

We will now look in more detail at the relationship between the seasonal variation of upper mesospheric temperatures and the occurrence rate of PMSEs and NLCs. The existence of these layers is critically determined by the degree of saturation $S = p_{H_2O}/p_{sat}$, where p_{H_2O} is the partial pressure of water vapor and p_{sat} is the saturation pressure of water vapor over ice as given by *Marti and Mauersberger* [1993]:

$$\log_{10} p_{sat} = 12.537 - (2663.5/T) \qquad (1)$$

where p_{sat} is in N/m^2 and T is in Kelvin. If S>1, the particles will grow, and if S<1, they will evaporate. In Figure 10 we show a contour plot of the degree of saturation as a function of altitude and season based on the temperature and density data in Tables 7 and 8, respectively. The water vapor mixing ratios required to determine p_{H_2O} were taken from the theoretical model of *Garcia and Solomon* [1994]. Typical mixing ratios (which are taken here to be independent of season) are 3.2, 2.4, and 1.6 parts per million by volume (ppmv) at altitudes of 80, 85, and 90 km respectively.

How does the seasonal variation of upper mesospheric temperatures and the degree of saturation compare with the PMSE and NLC occurrence? From the extensive record of the Poker Flat VHF radar data *Balsley and Huaman* [1997] have deduced PMSE occurrence ratios as a function of season (the latitude of Poker Flat, 65°N, is close to that of our launching site). Their statistics shows a gradual increase (decrease) in the beginning of June (mid-August) and a maximum of almost 100% around the beginning of July (see their paper for more details and a definition of occurrence ratios). Their summary curve is reproduced in Figure 10. Other radars have shown a similar seasonal variation of PMSE [e.g., *Bremer et al.*, 1996].

From the long and extensive record of visual NLC observations it is known that NLCs are most abundant at the beginning of July. From the cumulative occurrence frequency of M. Gadsden (private communication, 1998) we have derived an NLC occurrence probability distribution normalized to 100% for the time of maximum occurrence at the beginning of July. The seasonal variation of the relative occurrence is also shown in Figure 10. The NLCs and PMSEs distributions are rather similar and almost symmetrical around the peak in the beginning of July.

The time of year when the degree of saturation is larger than unity in Figure 10 roughly overlaps with the times when PMSEs and NLCs are observed. Particles can exist in the upper mesosphere (i.e., S>1) from the end of May until mid-August. The correlation be-

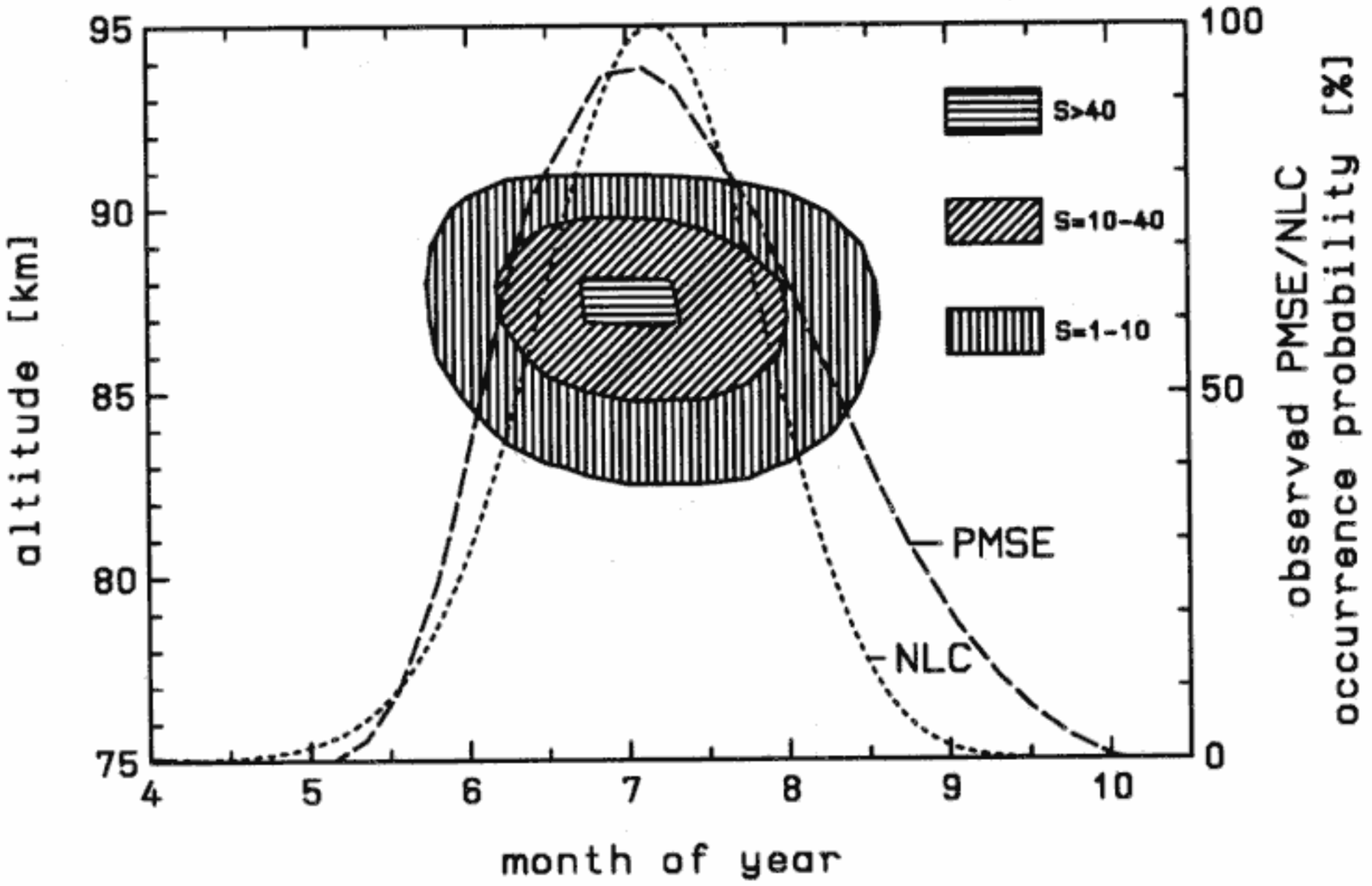

Figure 10. Contour plot of the degree of saturation S as a function of season and altitude (shaded areas). The range of S values corresponding to each shade pattern is given in the insert. S was determined using the FS temperatures from Table 7 and water vapor mixing ratios from *Garcia and Solomon* [1994]. Relative occurrence probability distributions (right axis) normalized to 100% at the maximum are given for PMSEs (dashed line) and for NLCs (dotted line). More details are explained in the text.

tween PMSE and NLC occurrence and the degree of saturation is more apparent if we study the variation of S with season at a given altitude, for example, around the mesopause (88 km), where the NLC and PMSE particles presumably start to nucleate before they grow and sediment to lower altitudes. As can be seen from Figure 11 the seasonal variation of S at 88 km closely matches the NLC and PMSE occurrence distribution, in particular, if we allow for some natural variability such that the actual temperatures are temporarily slightly smaller than our mean values. We note that there is still a significant chance to observe PMSEs in the beginning of September, when the temperature at 88 km is as high as 155 K. This implies that the atmosphere must have been colder by at least ~11 K during PMSE conditions to allow the ice particles to grow and exist (the water vapor mixing ratio would have to be ~120 ppmv to overcome the -11 K temperature difference, far more than available in the HLSM). We conclude that the thermal structure in the HLSM is the dominant factor controlling the existence of PMSEs and NLCs, whereas other parameters of importance for particle growth, such as condensation nuclei or water vapor, are of secondary importance. Significant deviations from the mean temperatures must temporarily exist in late August/early September to allow for the growth and existence of particles leading to PMSEs at this time of year.

Most of the NLCs occur at an altitude close to or above 82 km. This altitude has not changed significantly since the first discovery more than 100 years ago, which suggests that the thermal structure around this altitude is rather stable [*Lübken et al.*, 1996]. A recent survey of NLC and temperature measurements (including some of the profiles discussed above) has shown that the mean temperature at 82 km altitude during summer is persistently close to 150 K, an effect named "equithermal submesopause in summer" [*Lübken et al.*, 1996]. We have seen in Figure 6 that this temperature persists from June until mid-August. On the other hand, the degree of saturation at 82 km is smaller than unity during the entire summer (see Figure 10) and reaches maximum values of S=0.2-0.5 in mid-summer, which is too small for the particles to exist in the long run. This implies either that the mean water vapor mixing ratio at 82 km is at least twice as large as in the *Garcia and Solomon* [1994] model or (which seems more likely) that the temperature is 3–4 K lower during NLC conditions compared to the mean (see Figure 6).

When comparing the thermal structure and the NLC and PMSE occurrence in such detail, we should keep in mind that the particles require several hours to grow to visible size (perhaps less for PMSE particles) and that the nucleation process therefore has presumably started at horizontal distances of some hundreds of kilometers away from our launching site. In addition, we note that wave-like disturbances with vertical scales smaller than the resolution of the FS technique can be present in the upper atmosphere. Such waves might cool the atmosphere (at least locally and temporarily) below the freezing point of water vapor and could lead to aerosol

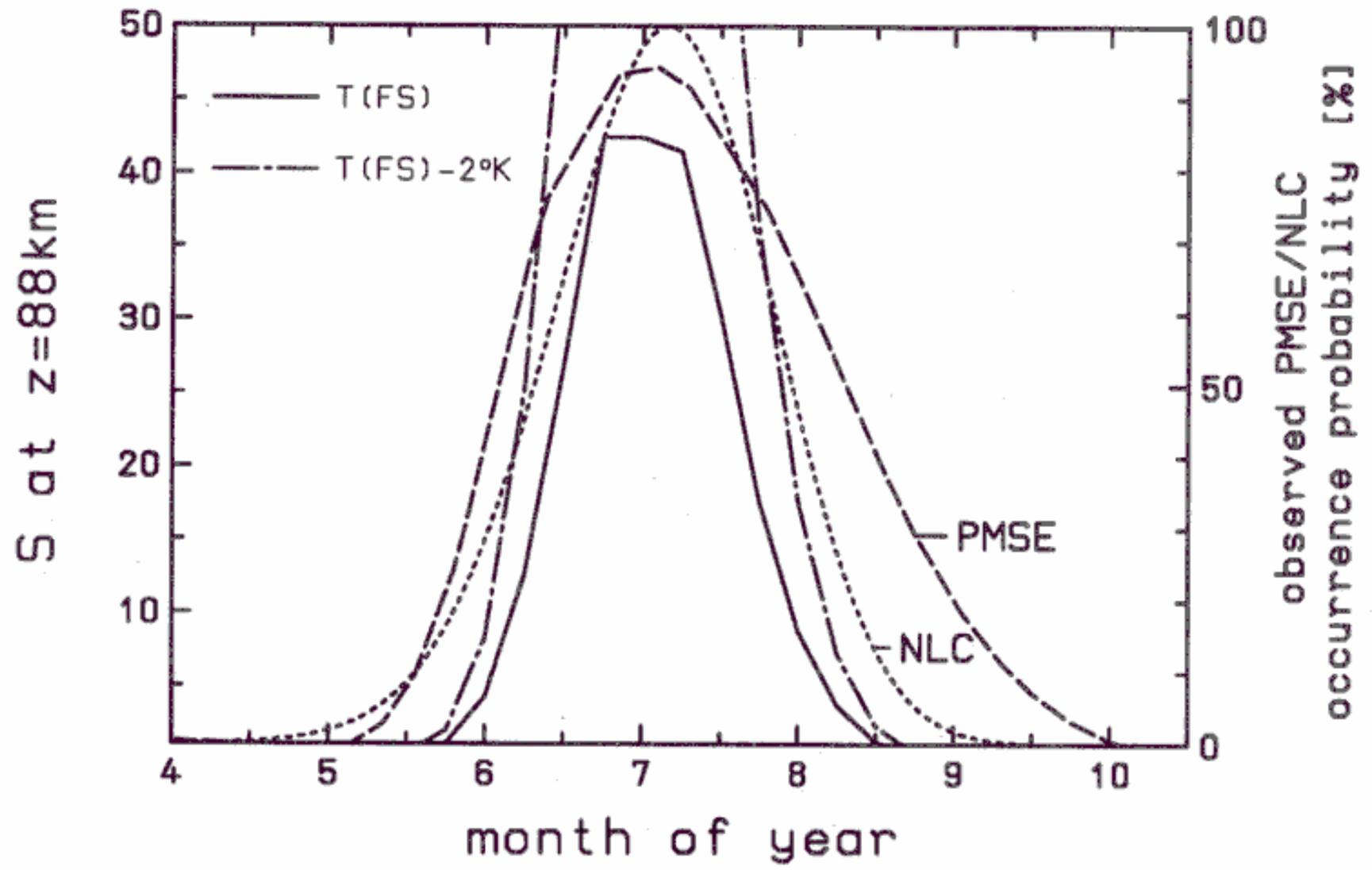

Figure 11. The degree of saturation (solid line) as in Figure 10 but shown at a fixed altitude of 88 km. In addition, the degree of saturation has been plotted using temperatures which are 2 K lower than those listed in Table 7 (dotted-dashed line). As in Figure 10 the PMSE (long-dashed line) and NLC (short-dashed line) occurrence distributions are shown for comparison.

particle formation. Detailed modeling of particle nucleation, growth, sedimentation, and charging is required to better understand the relationship between the thermal structure in the HLSM and the appearance of NLCs and PMSEs.

We have seen in Figure 8 that the temperatures in the upper mesosphere during summer are significantly lower compared to empirical models such as CIRA-1986 and MSIS-1990. Therefore conclusions on the NLC and PMSE seasonal variation based on these models must be taken with care and are most likely not appropriate [*Hall*, 1996; *Balsley and Huaman*, 1997].

6. Conclusions

From a total of 89 falling sphere flights performed during or close to the summer season in the last 10 years we have derived the seasonal variation of temperatures and densities at altitudes between 93 and 35 km in the polar middle atmosphere. The very cold summer mesopause with temperatures close to 130 K persists from mid-May until mid-August at 69°N latitude. The thermal structure in the Arctic mesosphere shows very little variability in that period. For example, at an altitude of 82 km (where lidars and ground-based observers frequently detect noctilucent clouds) the mean temperature changes by <4 K throughout the core summer months. Significant differences between the FS temperatures and empirical reference atmospheres were discovered. In addition, in the summer upper mesosphere the atmospheric mass densities derived from the FS flights are smaller by up to ~50% compared to CIRA-1986, which can play an important role, for example, when modeling particle sedimentation during PMSE and NLC conditions.

We find that the seasonal variation of NLCs and PMSEs nicely matches the seasonal variation of the degree of saturation S at the mesopause, whereas S is smaller than unity at 82 km during the entire summer season. This implies that NLC and PMSE particles cannot exist at this altitude in the long run. However, if the temperatures during NLC conditions are only 3–4 K lower compared to the mean, the degree of saturation is sufficiently large for the particles to survive. The thermal structure in the HLSM is consistent with the picture that the aerosol particles leading to NLCs and PMSEs start to nucleate around the mesopause and then sediment and grow until they approach the "high" temperatures of ~150 K at an altitude of ~82 km. We note that wave disturbances might (at least locally and temporarily) cool the atmosphere and therefore initiate particle nucleation at altitudes and times of year where the mean temperature would not support the nucleation of ice particles. Detailed modeling of particle nucleation and charging is required to fully understand the relationship between the thermal structure in the HLSM and the appearance of PMSEs and NLCs.

Acknowledgments. I am grateful to Stefanie Wong and Arno Müllemann for their support in analyzing the falling sphere flights. Helpful discussion and comments from K.-H. Fricke and U. von Zahn are appreciated. The excellent work by the crews of the Mobile Raketenbasis (Germany) and the Andøya Rocket Range (Norway) is gratefully acknowledged. The falling sphere flights were supported by the

Bundesministerium für Bildung, Wissenschaft, Forschung und Technologie, Bonn, under grants 50 OE 9201 and 50 EE 94010.

References

Alpers, M., T. Blix, S. Kirkwood, D. Krankowsky, F.-J. Lübken, S. Lutz, and U. von Zahn, First simultaneous measurements of neutral and ionized iron densities in the upper mesosphere, *J. Geophys. Res.*, *98*, 275–283, 1993.

Balsley, B. B., and M. Huaman, On the relationship between seasonal occurrence of northern hemispheric polar mesosphere summer echoes and mean mesopause temperatures, *J. Geophys. Res.*, *102*, 2021–2024, 1997.

Bremer, J., P. Hoffmann, A. H. Manson, C. Meek, R. Rüster, and W. Singer, PMSE observations at three different frequencies in northern Europe during summer 1994, *Ann. Geophys.*, *14*, 1317–1327, 1996.

Cho, J. Y. N., and J. Röttger, An updated review of polar mesosphere summer echoes: Observation, theory, and their relationship to noctilucent clouds and subvisible aerosols, *J. Geophys. Res.*, *102*, 2001–2020, 1997.

Fleming, E. L., S. Chandra, J. J. Barnett, and M. Corney, Zonal mean temperature, pressure, zonal wind, and geopotential height as functions of latitude, *Adv. Space Res.*, *10*(12), 11–59, 1990.

Forbes, J. M., Atmospheric tides, 2, The solar and lunar semidiurnal components, *J. Geophys. Res.*, *87*, 5241–5252, 1982.

Gadsden, M., and W. Schröder, *Noctilucent Clouds*, Springer-Verlag, New York, 1989.

Garcia, R. R., and S. Solomon, A new numerical model of the middle atmosphere, 2, Ozone and related species, *J. Geophys. Res.*, *99*, 12,937–12,951, 1994.

Goldberg, R., E. Kopp, G. Witt, and W. Swartz, An overview of NLC-91: A rocket/radar study of the polar summer mesosphere, *Geophys. Res. Lett.*, *20*, 2443–2446, 1993.

Hall, C. M., Spatiotemporal predictions of polar mesospheric summer echoes, *J. Geophys. Res.*, *101*, 23,491–23,498, 1996.

Hedin, A. E., Extension of the MSIS thermosphere model into the middle and lower atmosphere, *J. Geophys. Res.*, *96*, 1159–1172, 1991.

Hoffmann, P., W. Singer, D. Keuer, J. Bremer, and R. Rüster, Mean diurnal variations of PMSE as measured with the ALOMAR SOUSY radar during summer 1996, in *Proceedings of the 13th ESA Symposium on European Rocket and Balloon Programmes and Related Research, Öland, Sweden, Eur. Space Agency, Spec. Publ., ESA SP–397*, 471–475, 1997.

Lübken, F.-J., Aerodynamical effects in number density measurements in the lower thermosphere with the CONE instrument, *Adv. Space Res.*, *19*(1), 139–144, 1997a.

Lübken, F.-J., Seasonal variation of turbulent energy dissipation rates at high latitudes as determined by in situ measurements of neutral density fluctuations, *J. Geophys. Res.*, *102*, 13,441–13,456, 1997b.

Lübken, F.-J., and U. von Zahn, Thermal structure of the mesopause region at polar latitudes, *J. Geophys. Res.*, *96*, 20,841–20,857, 1991.

Lübken, F.-J., et al., Intercomparison of density and temperature profiles obtained by lidar, ionization gauges, falling spheres, datasondes, and radiosondes during the DYANA campaign, *J. Atmos. Terr. Phys.*, *56*, 1969–1984, 1994.

Lübken, F.-J., K.-H. Fricke, and M. Langer, Noctilucent clouds and the thermal structure near the Arctic mesopause, *J. Geophys. Res.*, *101*, 9489–9508, 1996.

Marti, J., and K. Mauersberger, A survey and new measurements of ice vapor pressure at temperatures between 170 and 250 K, *Geophys. Res. Lett.*, *20*, 363–366, 1993.

Schmidlin, F. J., The inflatable sphere: A technique for the accurate measurement of middle atmosphere temperatures, *J. Geophys. Res.*, *96*, 22,673–22,682, 1991.

Theon, J., W. Nordberg, L. Katchen, and J. Horvath, Some observations on the thermal behavior of the mesosphere, *J. Atmos. Sci.*, *24*, 428–438, 1967.

von Zahn, U., Achievements of ALOMAR, in *Proceedings of the 13th ESA Symposium on European Rocket and Balloon Programmes and Related Research, Öland, Sweden, Eur. Space Agency, Spec. Publ., ESA SP–397*, 141–159, 1997.

von Zahn, U., and W. Meyer, Mesopause temperatures in polar summer, *J. Geophys. Res.*, *94*, 14,647–14,651, 1989.

von Zahn, U., G. von Cossart, J. Fiedler, and D. Rees, Tidal variations of noctilucent clouds measured at 69° latitude by ground-based lidar, *Geophys. Res. Lett.*, *25*, 1289–1292, 1998.

Williams, P. J. S., G. O. Jones, J. R. Palmer, and H. Rishbeth, The association of polar mesosphere summer echo layers with tidal modes, *Ann. Geophys.*, *13*, 454–457, 1996.

F.-J. Lübken, Physikalisches Institut der Universität Bonn, Nussallee 12, 53115 Bonn, Germany. (e-mail: luebken@physik.uni-bonn.de).

(Received September 3, 1998; revised December 14, 1998; accepted December 22, 1998.)